ISSN 0915-633X

NATIONAL INSTITUTE FOR FUSION SCIENCE

Coupling to the Lower Hybrid Waves with the Multijunction Grill

K. Ohkubo and K. Matsumoto

(Received – Apr. 14, 1992)

NIFS-145 May 1992

RESEARCH REPORT
NIFS Series

NAGOYA, JAPAN

Coupling to the Lower Hybrid Waves with the Multijunction Grill

Kunizo OHKUBO and Kazunori MATSUMOTO*

National Institute for Fusion Science, Nagoya 464-01, Japan

**Toyama Prefectural University, Imizugun, Toyama 939-03, Japan*

(Received

Abstract: *Coupling characteristics of the multijunction grill have been studied theoretically and experimentally by using a multireflection method with the aid of scattering matrices not only at the junction plane but also at the grill mouth. The global reflection coefficients in the primary waveguide and secondary wave-guides can be estimated from the vector sum of reflecting components caused by each reflection between two scattering planes. The experimental results of scattering matrices and the global coupling agree well with calculated ones. It is shown that the multiple reflection in secondary waveguides of the four-junction grill for JIPPT-IIU tokamak is finished until three or four reflections. The length of the secondary waveguides is confirmed to be one of parameters determining the grill efficiency.*

KEYWORDS: multijunction grill, RF coupling, lower hybrid wave, scattering matrix, multiple reflection.

§1. Introduction

In the recent devices for fusion research, high-power microwaves have been increasingly used in the heating and current drive of plasma. At present, most antennas for RF heating and current drive adopt the phased array system to improve the heating efficiency of the plasma and the current driving efficiency by plasma waves where such improvement is in the form of lower hybrid waves and the ion cyclotron range of frequency. For the lower hybrid current drive (LHCD) Moreau and N'guyen[1] proposed a new grill coupler with a simple structure, i.e. the multijunction grill. This coupler has great advantage to the large tokamak from view point of cost efficiency. This new launcher was tested on the experiments of lower hybrid ion heating in the Petula-B tokamak[2]. The experimental results on both the heating efficiency and power reflection coefficient are similar to that of a conventional grill. Following experiments[3] on the same machine, by using a multijunction-modulus grill, showed the very low power-reflection coefficient less than 3%; this is known as a self-adaptation property. Recently, high power current drive experiments on JT-60 have been performed by exchanging a conventional grill launcher for a multijunction-modulus grill and encouraging results have been obtained[4].

The original theoretical investigation[1] on the multijunction grill was presented by Moreau and N'guyen with the scattering matrix at the junction plane and the reflection coefficient at the grill mouth. They assumed the reflection at the grill mouth is approximately represented by a coefficient with not a matrix but a complex constant, because the number of secondary waveguides is large enough. According to their theory, Litaudon and Moreau[5] investigated numerically coupling properties of a multijunction-modulus grill for the LHCD experiments on JET.

Preinhaelter[6] also studied this subject by other analytical method, not using a scattering matrix, and determined all forward and reflected waves both in the primary and secondary waveguides by the continuity conditions of the electric and magnetic fields at the junction plane and the grill mouth.

For a design of the multijunction grill with small number of secondary waveguides such as in small tokamaks, it is necessary to calculate all the scattering coefficients including the grill

mouth, when one modifies Moreau and N'guyen's method. In this paper, we formulate a simple coupling theory of the multijunction grill for any number of secondary waveguides and compare numerical calculation with experimental results for a four-junction grill designed for the JIPP-TII-U tokamak.

In §2, we describe a method to analyze coupling properties of the multijunction grill on the basis of scattering matrices both at the junction and the mouth, and of a phase shift matrix which indicates each phase change during a reflection between the grill mouth and the junction. In §3, we present results of numerical calculation with respect to the scattering matrix at the mouth facing the plasma with a step and ramp density profile, and to forward and reflected electric fields, loci of these fields in the complex-coordinates, power spectrum and directivity. In §4, details of experimental results accompanying the theoretical comparison are described about the scattering coefficients at the mouth and the dependence of coupling characteristics on the length between the junction and the mouth. A summary is presented in §5.

§2. Method of coupling analysis

2.1 Global coupling characteristic of multijunction grill

A multijunction grill is schematically shown in Fig.1, which is obtained by dividing the main waveguide into a given number of secondary waveguides by inserting metallic walls perpendicularly to the electric field. The phasing between adjacent secondary waveguides is usually made by inserting step phase-transformers in the secondary waveguides. By increasing the waveguide height of the transformer, the phase of a wave passed through the transformer changes owing to a increase of the wavelength in that part. In our experiments described in §4, the phasing is easily obtained by directly changing the length of each secondary waveguide because each secondary waveguide has a window. In the analytic treatment, the evanescent modes at both ends of the secondary waveguides are ignored. Here, we have studied the coupling properties by calculating the scattering coefficients of waves at the mouth, referring the previous analysis[7].

Let denote a scattering matrix at the junction plane by S, of which components is given

in §2.2, incident waves propagating forward to the junction by $A^{(k)}$, and scattering waves reflecting from the junction by $B^{(k)}$ at k-th multiple reflection. The matrices $A^{(k)}$ and $B^{(k)}$ are related by a linear transformation[8], when the number of the secondary waveguides is n;

$$\begin{bmatrix} B_0^{(k)} \\ B_1^{(k)} \\ \cdot \\ \cdot \\ B_n^{(k)} \end{bmatrix} = \begin{bmatrix} S_{00} & S_{01} & \cdot & & S_{0n} \\ S_{10} & S_{11} & \cdot & & S_{1n} \\ \cdot & \cdot & \cdot & S_{pq} & \cdot \\ \cdot & \cdot & \cdot & & \cdot \\ S_{n0} & S_{00} & \cdot & & S_{nn} \end{bmatrix} \begin{bmatrix} A_0^{(k)} \\ A_1^{(k)} \\ \cdot \\ \cdot \\ A_n^{(k)} \end{bmatrix} \quad (1)$$

where the subscript 0 of $B^{(k)}$ and $A^{(k)}$ indicates the primary waveguide and the subscript p (=1,..n) refers to the p-th secondary waveguide, as shown in Fig.1. The element S_{pq} shows a contribution to the p-th waveguide by an incident wave upon the q-th waveguide through scattering process.

In the case of k=1, only an incident wave upon the primary waveguide is nonzero, that is, $A_0^{(1)} \neq 0$, $A_1^{(1)} = \ldots = A_n^{(1)} = 0$. The above equation is simply written as

$$\begin{bmatrix} B_0^{(1)} \\ B_1^{(1)} \\ \cdot \\ \cdot \\ B_n^{(1)} \end{bmatrix} = \begin{bmatrix} S_{00} \\ S_{10} \\ \cdot \\ \cdot \\ S_{n0} \end{bmatrix} A_0^{(1)} \quad (2)$$

Since the impedance between a power source and the primary waveguide is assumed to be matched, no scattering wave back to the power source reflects again forward to the junction plane. After the second reflection, incident waves upon the primary waveguide are all zero, $A_0^{(k)} = 0 \quad (k \geq 2)$.

For $k \geq 2$, the linear transformation expressed by Eq.(1) is reduced to

$$\hat{B}^{(k)} \equiv \begin{bmatrix} B_1^{(k)} \\ \cdot \\ \cdot \\ B_n^{(k)} \end{bmatrix} = \begin{bmatrix} S_{11} & \cdot & & S_{1n} \\ \cdot & \cdot & & \cdot \\ \cdot & \cdot & & \cdot \\ S_{1n} & \cdot & & S_{nn} \end{bmatrix} \begin{bmatrix} A_1^{(k)} \\ \cdot \\ \cdot \\ A_n^{(k)} \end{bmatrix} \equiv \hat{S}\hat{A}^{(k)}$$

$$B_0^{(k)} = \begin{bmatrix} S_{01} & \cdot & & S_{0n} \end{bmatrix} \hat{A}^{(k)} \equiv \hat{s}\hat{A}^{(k)} \tag{3}$$

On the other hand, a similar relation is obtained at the grill mouth facing a plasma. We denote a scattering matrix at the grill mouth by T, incident waves propagating forward to the mouth by $a^{(k)}$, and scattering waves reflecting from the mouth by $b^{(k)}$ at k-th multiple reflection. The matrices $a^{(k)}$ and $b^{(k)}$ are related by

$$\begin{bmatrix} b_0^{(k)} \\ b_1^{(k)} \\ \cdot \\ \cdot \\ b_n^{(k)} \end{bmatrix} = \begin{bmatrix} T_{00} & T_{01} & \cdot & & T_{02} \\ T_{10} & T_{11} & \cdot & & T_{1n} \\ \cdot & \cdot & T_{pq} & & \cdot \\ \cdot & \cdot & \cdot & & \cdot \\ T_{n0} & T_{n1} & \cdot & & T_{nn} \end{bmatrix} \begin{bmatrix} a_0^{(k)} \\ a_1^{(k)} \\ \cdot \\ \cdot \\ a_n^{(k)} \end{bmatrix} \tag{4}$$

where the subscript 0 denotes a plasma. We assume that no wave reflects from the plasma core toward the mouth, $a_0^{(k)} = 0$. As we are interested in coupling characteristics of the multijunction grill, we deal with only components concerning secondary waveguides. Consequently, Eq.(4) reduces to

$$\hat{b}^{(k)} \equiv \begin{bmatrix} b_1^{(k)} \\ \cdot \\ \cdot \\ b_n^{(k)} \end{bmatrix} = \begin{bmatrix} T_{11} & \cdot & & T_{1n} \\ \cdot & \cdot & & \cdot \\ \cdot & \cdot & & \cdot \\ T_{n1} & \cdot & & T_{nn} \end{bmatrix} \begin{bmatrix} a_1^{(k)} \\ \cdot \\ \cdot \\ a_n^{(k)} \end{bmatrix} \equiv \hat{T}\hat{a}^{(k)} \tag{5}$$

When a wave propagates between the junction and the mouth, its phase increases. The incident waves $\hat{a}$ into the mouth and $\hat{A}$ into the junction are expressed by

$$\hat{a} = \begin{bmatrix} \Phi_{11} & 0 & . & 0 \\ 0 & \Phi_{22} & . & 0 \\ . & . & \Phi_{pp} & . \\ 0 & . & . & \Phi_{nn} \end{bmatrix} \hat{B}^{(k)} \equiv \hat{\Phi}\hat{B}^{(k)} \tag{6-1}$$

$$\hat{A} = \hat{\Phi}\hat{b}^{(k)} \quad , \tag{6-2}$$

where $\hat{\Phi}$ is a diagonal matrix defining the phase shift. The phase shift in the p-th secondary waveguide is given by

$$\Phi_{pp} = exp\{j[k_g L + (p-1)\Delta\phi]\}, \tag{7}$$

where L is a length of the secondary waveguide, k_g is a wavenumber and $\Delta\phi$ is the phasing between adjacent waveguides. Substituting $\hat{a}$ and $\hat{A}$ into Eqs.(5) and (3), respectively, one has

$$\hat{b}^{(k)} = \hat{T}\hat{\Phi}\hat{B}^{(k)} \quad , \tag{8-1}$$

$$\left.\begin{aligned} \hat{B}^{(k)} &= \hat{S}\hat{\Phi}\hat{b}^{(k)}, \\ B_0^{(k)} &= \left[S_{01} \cdot \quad S_{0n}\right]\hat{\Phi}\hat{b}^{(k)} \equiv \hat{s}\hat{\Phi}\hat{b}^{(k)}, \end{aligned}\right\} \quad (\text{for } k \geq 2) \tag{8-2}$$

where $B_p^{(1)} = S_{p0}A_0^{(1)}$ $(p \geq 0)$ is given by Eq.(2). All the components can be iteratively calculated by the equations.

The global reflection coefficient in the primary waveguide is calculated by the ratio of total reflecting wave to the incident one,

$$\Gamma_0 = \frac{\sum_{k=1}^{\infty} B_0^{(k)}}{A_0^{(1)}} \tag{9-1}$$

Similarly, the reflection coefficient in the p-th secondary waveguide at the mouth is obtained by

$$\Gamma_p = \frac{\sum_{k=1}^{\infty} b_p^{(k)}}{\sum_{k=1}^{\infty} a_p^{(k)}} \qquad (p = 1,...n) \tag{9-2}$$

It is worth while to indicate that the summation means vector addition.

2.2 Scattering coefficients

At first, we refer to scattering matrix S at the E-plane junction, whose general expressions

have been given by Moreau and N'guyen[1]. When we consider only the dominant mode both in the primary and secondary waveguides, theoretical scattering coefficients are simply expressed as

$$\left.\begin{aligned} S_{00} &= -\frac{x-n}{x+n} \quad , \\ S_{p0} &= S_{0p} = -\frac{2\sqrt{x}}{x+n} \quad , \qquad \text{for} \quad p \neq 0 \end{aligned}\right\} \tag{10-1}$$

$$S_{pq} = \begin{cases} 1-\dfrac{2}{x+n} \ , & \text{for} \quad p = q \\ -\dfrac{2}{x+n} \ , & \text{for} \quad p \neq q \end{cases} \tag{10-2}$$

where $x=W/w$ is a ratio of the primary waveguide width W to the secondary one w and n is the number of secondary waveguides. It is noted that the scattering coefficients satisfy the conservation of energy, $\sum |S_{pq}|^2 = 1$.

Second, we calculate scattering matrix $\hat{T}$ at the mouth by a simplified conventional gill theory[7] where higher modes are ignored. The grill is assumed to be infinitely high and the grill edge to be connected with the conducting infinite wall. The density profile in front of the mouth is modelled by the step(n_{wgd}) plus ramp(∇n_{wgd})[9]. When an incident wave is injected only to the m-th waveguide, a scattered electric field E_{rq} normalized with the incident field E_{im} at the q-th waveguide is given by

$$\sum_{q=1}^{n} (w_p \delta_{pq} + U_{pq})\, T_{qm} = w_p \delta_{pm} - U_{pm} \quad , \tag{11-1}$$

$$T_{qm} = \frac{E_{rq}}{E_{im}} \quad , \tag{11-2}$$

$$\delta_{pq} = \begin{cases} 0 & (p \neq q) \\ 1 & (p = q) \end{cases} , \qquad \delta_{pm} = \begin{cases} 0 \ , & (p \neq m) \\ 1 \ , & (p = m) \end{cases} , \tag{11-3}$$

where T_{qm} indicates a scattering coefficient which connects the q-th waveguide to the m-th one, w_p is a p-th waveguide width and U_{pm} is written by

$$U_{pm} = \frac{1}{y_0}\int_{-\infty}^{\infty} y_{pl}\frac{2}{\pi N_z^2}\sin\left(\frac{N_z w_p}{2}\right)\sin\left(\frac{N_z w_m}{2}\right) e^{jN_z(\zeta_p-\zeta_m)}\, dN_z \quad , \qquad (12)$$

where y_0 is the admittance in a vacuum, y_{pl} is the surface admittance of a plasma, N_z is the refractive index along the magnetic field, ζ_p and ζ_m are positions of the p-th and m-th waveguides, normalized to the inverse free-space wavenumber, respectively. We can write y_{pl} as, for $|N_z| < 1$,

$$y_{pl} = \frac{-jy_0}{(1-N_z^2)^{2/3}}\frac{A'_i(\eta)}{A_i(\eta)}\left(\frac{\nabla n_{wgd}}{n_c}\right)^{1/3} \quad , \qquad (13\text{-}1\text{-}1)$$

$$\eta = (1-N_z^2)^{1/3}\left(\frac{\nabla n_{wgd}}{n_c}\right)^{-2/3}\left(\frac{n_{wgd}}{n_c}-1\right) \quad , \qquad (13\text{-}1\text{-}2)$$

and for $|N_z| > 1$,

$$y_{pl} = \frac{-jy_0}{(N_z^2-1)^{2/3}}\frac{A'_i(\eta)+jB'_i(\eta)}{A_i(\eta)+jB_i(\eta)}\left(\frac{\nabla n_{wgd}}{n_c}\right)^{1/3} \quad , \qquad (13\text{-}2\text{-}1)$$

$$\eta = -(N_z^2-1)^{1/3}\left(\frac{\nabla n_{wgd}}{n_c}\right)^{-2/3}\left(\frac{n_{wgd}}{n_c}-1\right) \quad , \qquad (13\text{-}3\text{-}1)$$

where n_c is the critical density of the electron plasma wave with the frequency of the injected RF, n_{wgd} and ∇n_{wgd} are the electron density and its density gradient just in front of the mouth. Here, A_i, B_i, A'_i and B'_i are Airy functions and their first derivatives, respectively. It is worth while to note that when we numerically integrate Eq.(12) over N_z, we can introduce a new variable of the integration u in order to avoid the singularity at N_z=1: for $|N_z| < 1$, N_z=1-u^3, for $|N_z| > 1$, N_z=1+u^3.

§3. Numerical Calculation

3.1 Scattering coefficients at the grill mouth

In order to examine antenna-plasma coupling properties, numerical calculations of forward and reflected electric fields both in the primary waveguide and the secondary ones are carried out for a multijunction grill designed for LHCD experiments in the JIPP T-IIU tokamak[7].

The grill has four secondary waveguides with the equal widths, whose mouth is the same as the conventional grill used for the previous experiments[7]. The width w of the secondary waveguide is 3.5cm and the thickness d of the septum is 0.5cm; the width W of the primary waveguide is 15.5cm. The RF frequency of the oscillator is 800MHz whose critical density n_c is $7.9\times10^{9} cm^{-3}$.

Both phase and amplitude of scattering coefficients of the first and second row matrix elements, T_{p1} and T_{p2}, are plotted as functions of n_{wgd}/n_c in Figs.2(a), (b), (c) and (d), respectively, where $\nabla n_{wgd}=1\times10^{11} cm^{-4}$. Since the mouth is geometrically symmetry, there are relations of $T_{13}=T_{42}$, $T_{23}=T_{32}$, $T_{33}=T_{22}$, $T_{43}=T_{12}$, $T_{14}=T_{41}$, $T_{24}=T_{31}$, $T_{34}=T_{21}$ and $T_{44}=T_{11}$. Matrix components of T_{p3} and T_{p4} are obtained by T_{p1} and T_{p2}.

It is found that both amplitude and phase of self-scattered component T_{11}(T_{22}) is sensitive to the variation of the density in front of the grill. The optimum density, where $|T_{11}|$ ($|T_{22}|$) is minimum and the phase changes considerably, is approximately expressed[7] by $n_{wgd} \approx n_c N_z^2$. As for mutual components T_{p1} (T_{p2}) scattered from the launching waveguide, the amplitudes as shown in Fig.2(b) (Fig. 2(d)) become gradually smaller as being apart from the launching waveguide; $|T_{21}|>|T_{31}|>|T_{41}|$ ($|T_{12}| = |T_{32}|>|T_{42}|$). The phase $\angle T_{21}$ ($\angle T_{42}$) adjacent to the launching waveguide is nearly out of phase. Absolute values of the phase decrease as being apart from the source; $\angle T_{21}|>|\angle T_{31}|>|\angle T_{41}|$ ($|\angle T_{12}| = |\angle T_{32}|>|\angle T_{42}|$).

It may be worth while to indicate that there is a slight difference between the coefficients $T_{12}(T_{42})$ and $T_{21}(T_{31})$, which results from the boundary configuration of the grill.

3.2 Coupling characteristics

The amplitude and the phase of forward and reflected waves at the mouth in the No.2 secondary waveguide are plotted as functions of n_{wgd}/n_c in Figs.3(a), (b), (c) and (d), respectively. Those of the reflected wave at the junction plane in the primary waveguide are plotted in Figs.3(e) and 4(f). Here $\Delta\phi=90°$, $\nabla n_{wgd}=1\times10^{11} cm^{-4}$, and thin solid curves show results for $k_gL=30°$ and broken curves for $k_gL=150°$. The parameter k_gL is the length of the secondary waveguide normalized to the inverse wavenumber in the waveguide. The subscript 0 of E indicates the primary waveguide and 2 does the No.2 secondary waveguide. The subscript i and

r indicate the forward and reflected wave, respectively.

The forward electric field at the primary waveguide is $2\angle 0°$ and corresponding forward waves for the equivalent conventional four-waveguide grill are $1\angle 0°$, $1\angle 90°$, $1\angle 180°$ and $1\angle 270°$. Thick solid curves shown in Fig.3(d) and (f) indicate amplitude of reflected waves for the equivalent conventional grill, where the amplitude to be compared with $|E_{r0}|$ is calculated from the square root of the total reflected power in the conventional grill.

In Fig.3(f), $|E_{ro}|$ in the primary waveguide has a minimum value for $k_gL=30°$ near $n_{wdg}/n_c=20$ where $\angle E_{r0}$ changes remarkably as shown in Fig.3(e). On the contrary, in Fig.(d), a minimum $|E_{r2}|$ in the No.2 secondary waveguide is obtained for $k_gL=150°$ near $n_{wgd}/n_c=5$ where $\angle E_{r2}$ undergoes a considerable phase change as shown in Fig.3(c). These results indicate that the coupling property of the multijunction grill strongly depends on k_gL and that the length of the secondary waveguide is one of important parameters for grill design.

In Fig.3(b), $|E_{i2}|$ for both $k_gL=30°$ and 150° are larger than unity for almost whole range of n_{wgd}/n_c. This behavior is quite distinct from the equivalent conventional grill. In Fig.3(a), $\angle E_{r2}$ has a value of -250° ~ -215° for $k_gL=30°$ and -125° ~ -140° for $k_gL=150°$, which is considerably different from that imposed by phasing, -270° (=360°-$\Delta\phi$): phasing is scrambling by multiple reflection between the mouth and the junction.

The thick solid curve in Fig.3(f) indicates that the reflected field corresponding to the equivalent conventional grill has a large value compared with those of the multijunction grill. The feature known as a self adaptation property[1] is found in Fig.3(b), (d) and (f).

In order to understand coupling characteristics of the multijunction grill clearly from the view point of multiple reflection, we plot the loci both of the forward and reflected fields at the mouth in each secondary waveguide in the complex co-ordinates. Forward and reflected fields are plotted in Fig.4(a) and (b), where the number written in a square box indicates the secondary waveguide number, $k_gL=90°$, $\Delta\phi=90°$, $n_{wgd}/n_c=31.6$ and $\nabla n_{wgd}=1\text{x}10^{11}cm^{-4}$. Vectors marked with 1st, 2nd and 3rd show the first, second and third forward (reflected) components for (from) the mouth. The forward electric field at the primary waveguide is $2\angle 0°$ and corresponding forward waves for the equivalent conventional four-waveguide grill are $1\angle 0°$, $1\angle 90°$,

$1\angle 180°$ and $1\angle 270°$. Here, it is worth while to note in Fig.4(b) that each 1st vector corresponds to a reflected electric field of each waveguide in the conventional grill.

In Fig.4(a), each tip of 1st forward vector is located closely on the unity circle and the angles are separated by 90°. The amplitude and phase of each 1st vector of the secondary waveguide , scattered from the primary waveguide at the junction, are calculated at 0.95 and 0° from Eq.(10-1). Its phase in the p-th waveguide at the mouth is done at $90°p$ from Eq.(7) for k_gL=90° and $\Delta\phi$=90°. It should be noted that the phasing of the 2nd vector or 3rd vector no longer satisfy $\Delta\phi$=90°, since forward vectors into the mouth are reflected according to complex scattering coefficients with different values. Therefore, the power spectrum which may not contribute a current drive is excited by these components.

It is seen explicitly in Fig.4(a) and (b) that variations of the forward and reflected fields in the secondary waveguide are caused by multiple reflection. The waves are considerably diminished by launching the power to plasma and disappear after 3rd or 4th reflection at the mouth. When the plasma load is not so matching with the antenna, however, enhanced reflections occur.

Let consider the effect of the length of the secondary waveguide, k_gL, on the loci of the multi-reflected waves. Loci of forward fields in the No.2 secondary waveguide at the mouth and of reflected fields in the primary waveguide at the junction plane are shown for various k_gL in Fig.5(a) and (b), respectively, where $\Delta\phi$=90°, n_{wgd}/n_c=31.6 and ∇n_{wgd} =1×10^{11}cm^{-4}. In Fig.5(a), a vector of the 1st forward component rotates proportionally to the amount of the angle k_gL, but those beyond 2nd components do not behave as the 1st component; each vector rotates by a various angle on the tip of each mother vector. Therefore, it is found that the discrepancy among rotation angles of higher reflected vectors causes the field variation in the waveguide with respect to k_gL. An enhanced or suppressed field in comparison with the field in conventional grill is excited in the secondary waveguides according to k_gL. If we consider precisely the phase change of a reflected wave through a trip as to k_gL, we get that the angle of 2nd vector changes to the amount of k_gL+$2k_gL$ and k-th one does to $k_gL + \sum_{m=1}^{k-1} 2mk_gL$. The result shown in Fig.5(b), which presents the behavior of the reflected wave for the primary waveguide at the junction plane as to k_gL, can be also understood by the above-mentioned interpretation. But the

starting point of the vectors is different from that in Fig.5(a), which is marked by a open circle. As Eq.(10-1) indicates, it comes from that an incident wave departing from a wave source is reflected by the septum of the junction. It should be mind that the reflection coefficient in the primary waveguide varies depending strongly on k_gL.

Fig.6(a) illustrates schematically how a multijunction-grill field E changes with k_gL, where we assume E is roughly expressed by vector addition of only 1st and 2nd components, $E^{(1)}$ and $E^{(2)}$ for simplicity. When the value of k_gL changes by $k_g\Delta L$, the phase of $E^{(1)}$ changes by the same amount of angle, but that of $E^{(2)}$ with a initial phase ϑ does by 3 $k_g\Delta L$. For instance, if $E^{(1)}$ is rotated clockwise by 90°, $E^{(2)}$ by 270°. Therefore, the amplitude of E is modulated nearly sinusoidally by the change of k_gL, as shown in Fig.6(c), whose curve is dependent on ϑ. Furthermore, it is found in Fig.6(b) that if the amplitudes beyond 2nd components are not so small compared with that of the 1st one, the phase of E does not change proportionally to the variation of k_gL and its curve is dependent on ϑ.

The items of criteria of optimization for launcher design are the directivity of the antenna and the global power reflection coefficient in the primary waveguide. The maximum electric field generated in the secondary waveguides is also important for power transmission without a breakdown. Reflection coefficient in the primary waveguide and the directivity of the power spectrum radiated from the mouth are plotted as functions of phasing between adjacent secondary waveguide for various k_gL in Fig.7(a) and 7(b), respectively, where a bold solid curve is calculated from the equivalent conventional grill, n_{wgd}/n_c=10 and ∇n_{wgd} =1x$10^{11}cm^{-4}$. Here, directivity of launching wave is estimated by $\int_1^{\infty} P(N_z)\,dN_z / \int_{-\infty}^{\infty} P(N_z)\,dN_z$; strictly speaking, the lower limit of the integration should be determined from the accessibility condition. Fig.7(a) presents that the amplitude of the reflection coefficient in the primary waveguide is always small for any pair of k_gL and $\Delta\phi$ in comparison with the one in the conventional grill, which indicates the self-matching property of the multijunction grill. In the same figure, $|\Gamma_0|$ oscillates at a fairly regular interval with respect to $\Delta\phi$. For instance, $|\Gamma_0|$ becomes very small for $\Delta\phi$≈45° and 135° in k_gL=0. This result can be explained as follows. As described in the numerical results (Fig.5(b)), a field reflected for the primary waveguide is roughly determined by the 1st and 2nd forward waves onto the junction plane. So, we consider only these components, i.e. $A_p^{(1)}$ and

$A_p^{(2)}$ shown in Fig.1. We assume that the scattering at the grill mouth is simply expressed by a reflecting coefficient in order to understand the result qualitatively. Then, at $\Delta\phi$=45° and 135°, components of the 1st vector, $A_p^{(1)}$ (p=1,..4), have a same amplitude and 90° phase difference between adjacent components. The values of $A_p^{(2)}$ (p=1,..4) have a same amplitude and 180° phase difference between adjacent components. It is found from Eq.(10-1) for S_{op} that the total scattering wave into the primary waveguide is zero for both $A_p^{(1)}$ and $A_p^{(2)}$. Therefore, we get a very small reflection coefficient at $\Delta\phi$=45° and 135° for k_gL=0.

Fig.7(b) indicates that the directivity of the launched power spectrum is not always improved as compared with the one of the conventional grill, though the power launched into a plasma increases by virtue of the reduction of the reflection coefficient in the primary waveguide. The directivity becomes 0.5 for $\Delta\phi$=0° or 180° because of power-spectrum symmetry for N_z. The directivity changes remarkably with k_gL at a relatively small $\Delta\phi$, where power spectrum variations are examined as shown in Fig.8.

Power spectra of waves radiated from the multijunction grill into the plasma are shown for $\Delta\phi$=30° in Fig.8, where a solid curve is the calculation for the conventional grill and other parameters are the same with ones in Fig.7(a) and (b). The integral value of $P(N_z)$ over whole N_z becomes always large as compared with that of conventional grill owing to the increase of the launched power for any k_gL and $\Delta\phi$, as indicated in Fig.7(a). It is seen that as k_gL increases, $P(N_z)$ extends to a large positive N_z region, then $P(N_z)$ has parasitic peaks both in wide positive and negative N_z regions. These variation in $P(N_z)$ leads to the change in directivity, as shown in Fig.7(b). The reason why $P(N_z)$ extends to large N_z region and has parasitic peaks as the increase in k_gL is that the phasing among multi-reflected components at the mouth increases.

§4. Experiments

4.1 Method and device

The experiments are carried out in the JIPPT-IIU tokamak by injecting the low power (< 1*W*) RF of 800*MHz* via the multijunction grill. Any phasing between adjacent secondary waveguides is adjusted by directly changing the length of each secondary waveguide, which is

thought to be a suitable experimental method to investigate in detail the effect of the phasing and length on the coupling property. Two kinds of extra waveguides are inserted into each secondary waveguide by using waveguide-bends; one is for a phasing which is consist of four waveguides with different lengths corresponding phasing to be set, and the other is waveguides with equal length to examine the coupling effect of $k_g L$.

To measure amplitude and phase of forward and reflected fields with the frequency of $800MHz$, four special directional couplers[10] are installed on each secondary waveguide. To monitor indirectly those in a primary waveguide, the coaxial directional coupler (HP778D) are inserted before the primary waveguide. The every element of scattering matrices both at the junction and the mouth are directly estimated by the method of wave packet injection[11] which was designed for directly determining the scattering coefficients. The wave packet with typically $10ns$ duration of $800MHz$ frequency is applied to one of the primary or secondary waveguides, then the wave packets scattered into every waveguide are detected by the above directional couplers. Since the detection is finished before the reflected wave packet at the end of the outlet arrives again, this wavepacket-injection technique needs no matched termination at any waveguides as conventional methods[12].

4.2 Scattering coefficients

Table I shows the first and second column elements of the scattering matrix at the junction plane, which are measured by the wavepacket method[11] and calculated by Eqs.(10-1) and (10-2), respectively. We find a good agreement between the experimental and theoretical values. It is worth while to indicate that since the sign of S_{00} and $S_{12}(S_{32}, S_{42})$ are minus, their scattered waves are out of phase to the incident wave.

Amplitude and phase of the first column elements of the matrix $\hat{T}$ at the mouth facing a plasma whose density is an order of magnitude larger than a usual LHCD experiment are shown in Fig.9(a) and (b), respectively. Those of the secondary column are shown in Fig.9(c) and (d), where open circles indicate experimental values, dots are theoretical ones which are connected by lines for convenience. Experimental results agree well with the calculated values estimated at n_{wgd}/n_c=31.6 and ∇n_{wgd} =5x10^9~1x10$^{11}cm^{-4}$. It is exhibited experimentally that an ampli-

tude of a scattered wave becomes small as apart from the launching waveguide and the phase is almost out of phase. Here, we should be noted that the phase of a self-scattering component $T_{11}(T_{22})$ has a opposite sign to S_{22} at the junction.

4.3 Coupling characteristics

The coupling property is examined by launching a long RF pulse (~1μsec) into the multijunction, whose results can be regarded as CW; our analytical results expressed by Eq.(9-1) and (9-2) is applicable to CW. The experimental and calculated results of reflected amplitude $|E_{r0}|$ at the junction for the primary waveguide are shown as functions of k_gL in Fig.10(a) and (d), respectively and those of the amplitude of forward waves $|E_{ip}|$ and reflected waves $|E_{rp}|$ in the secondary waveguide at the mouth of multijunction are shown in Fig.10(b), (c) and (e), (f), respectively, where $\Delta\phi=30°$ and each amplitude is normalized to the amplitude of forward wave in the primary waveguide $|E_{i0}|$. To compare the results from experiments with calculations, the value of k_gL in experiments is set to zero where the $|E_{r1}|$ is minimum. Theoretical calculations are made under the same conditions as those in Fig.9. In Fig.10(b),(e),(c) and (f), open and solid circles, asterisk and triangle correspond to p=1, 2, 3 and 4 of secondary waveguide number.

The experimental results agree well with calculated values. Deviation of observed amplitudes from the calculated ones is considered to be resulted partly from the small disagreement between the observed scattering matrix at the grill mouth and calculated one. It is seen that almost all the amplitudes vary nearly sinusoidally with k_gL, whose mechanism is explained schematically in Fig.6(a) and (c).

Fig.10(a) and (d) indicate that reflection for the primary waveguide reaches a minimum when we choose the optimum length of secondary waveguide. It should be noted in Fig.10(b) and (e) that the amplitude imbalance of forward waves in the secondary waveguides occurs and that in the certain k_gL the amplitude has the value higher than 0.5 which is the value in the equivalent conventional grill.

We have measured not only the amplitude but also the phase of each observed wave as shown in Fig.11. Good agreement between the experiment and the calculation is also obtained. It is worth while to point out that the phase in every waveguide does not shift linearly with in-

creasing length of secondary waveguide, as one qualitatively understood in Fig.6(a) and (b).

When the 1st reflected vector at the mouth has a large amplitude as compared with ones of the other multi-reflected vectors, the phase change with respect to $k_g L$ becomes almost linear as the recent numerical results[5].

§5. Summary

We have developed a general analysis of the multijunction grill by using the scattering matrices both at the junction and at the grill mouth. The coupling properties estimated numerically have been compared in detail with the results obtained experimentally for the four-junction grill in the JIPPTII-U tokamak.

The scattering matrices at the junction and the mouth measured by the wavepacket method are in good agreement with the results calculated numerically. By examining numerically the loci of multi-reflected waves in the complex co-ordinates, we indicated explicitly that coupling variation is caused by the difference in the vector addition of each multi-reflected wave.

We have investigated the dependence of coupling characteristics on the length between the junction plane and the mouth. The results obtained by both numerically and experimentally are as follows:

(a) There exists a optimum length at which the reflection coefficient in the primary waveguide is minimum. (b) In stead of the reduced reflection in the primary waveguide, electric field intensities in some secondary waveguides increases fairly as compared with ones in the conventional grill. (c) Though a launched power to a plasma increases generally, the power spectrum changes from the one in the conventional grill and has clear parasitic peaks at a certain condition. The power directivity change drastically for small phasing.

The above results should be taken into consideration in designing a multijunction grill with small number of secondary waveguide.

Acknowledgments

The authors would like to express their thanks to Dr. T. Sato, Dr. Y. Hamada and Dr. T. Kuroda for their encouragement, and to the members of the RF group for their discussion.

One of the authors (K.M.) wishes to thank Prof. M. Sato and Prof. S. Ishii for their continuous supports. This work was done supported by a Grant-in-Aid for Scientific Research from the Ministry of Education, Science and Culture.

References

[1] D. Moreau and T.K. N'guyen: *Couplage de l'onde lente au voisinage de la fréquence hybrid basse dans les grands tokamaks*, Association Eurtom-CEA, Centre d'études nucléaires de Fontanay-aux-Roses, Dept. de la fusion controlée, Research Report EUR-CEA-FC-1246, (1983/1984).

[2] C. Gormezano, P. Briand, G. Briffod, G.T. Hoang, T.K. N'guyen, D. Moreau, G. Ray: Nucl Fusion **25** (1985) 419.

[3] M. Goniche, C. David, G. Tonon, G. Rey, P. Briand: Proc. 13th Eur. Conf. on Cont. Fusion and Plasma Heating, vol.**10c** part 2 (1986) 370.

[4] JT-60 Team: Plasma Phys. Controlled Fusion **31** (1989) 1579.

[5] X. Litaudon and D. Moreau: Nucl. Fusion **30** (1990) 471.

[6] J. Preinhaelter: Nucl. Fusion **29** (1989) 1729.

[7] K. Ohkubo and K. Matsumoto: Jpn. J. Appl. Phys. **26** (1987) 142.

[8] R. Chatterrjee: *Advanced Microwave Engineering, Special Advanced Topics* (Ellis Horwood Limited, Chichester, 1989).

[9] J. Stevens. M. Ono, R. Horton, J.R. Wilson: Nucl. Fusion **21** (1981) 1259.

[10] K. Ohkubo: J. Phys. E **16** (1983) 715.

[11] K. Ohkubo: Jpn. J. Appl. Phys. **30** (1991) L1212.

[12] R. Chatterrjee: *Advanced Microwave Engineering, Special Advanced Topics* (Ellis Horwood Limited, Chichester, 1989).

Table I Elements of scattering matrix S at junction plane, where CAL denotes theoretically calculated results from Eqs.(10-1, -2) and EXP does experimentally measured ones.

	S_{00}	S_{p0}	S_{02}	$S_{12}=S_{32}=S_{42}$	S_{22}
CAL	-0.039	0.499	0.499	-0.239	0.76
EXP	-0.05~-0.1	0.5~0.55	0.55	-0.27~-0.33	0.77

Figure Captions

Fig.1: Conceptual drawing of a multijunction grill.

Fig.2: The 1st and 2nd column elements of the scattering matrix $\hat{T}$ at the grill mouth facing the plasma as functions of edge density n_{wgd} normalized with critical density n_c as parameters of waveguide number p. (a) phases $\angle T_{p2}$ and (b) amplitudes $|T_{p2}|$ of 2nd column, (c) phases $\angle T_{p1}$ and (d) amplitudes $|T_{p1}|$ of 1st column. Here, w=3.5cm, d=0.5cm, W=15.5cm, f=800MHz and $\nabla n_{wgd}= 1 \times 10^{11} cm^{-4}$.

Fig.3: RF electric fields in primary and No.2 secondary waveguides as functions of normalized density n_{wgd}/n_c for two secondary waveguide lengths of k_gL=30° (solid curve) and k_gL=150° (dashed curve). (a) phases and (b) amplitudes of forward electric fields in No.2 secondary waveguide, (c) phases and (d) amplitudes of reflected fields in the same secondary waveguide, (e) phases and (f) amplitudes of reflected fields in primary waveguide. Here, forward field in the primary waveguide $|E_{i0}|$ is set to $2\angle 0°$ and bold solid curves indicate the results for the equivalent conventional grill. Here, w=3.5cm, d=0.5cm, W=15.5cm, f=800MHz and $\nabla n_{wgd}=1 \times 10^{11} cm^{-4}$.

Fig.4: Loci of multiply reflected electric fields of secondary waveguides at the grill mouth in the complex co-ordinates: (a) forward fields, (b) reflected fields, where vectors denoted by 1st (2nd, 3rd) indicates an incident component arrived at the grill mouth for the first (second, third) time and waveguide number is written in a square box. Since we define $|E_{i0}|= 2\angle 0°$, forward vectors for the equivalent conventional grill takes their positions on a circle with a radius of 1 in figure (a). Here, w=3.5cm, d=0.5cm, W=15.5cm, f=800MHz, k_gL=90°, $\Delta\phi$=90°, n_{wgd}/n_c=31.6 and $\nabla n_{wgd}= 1 \times 10^{11} cm^{-4}$.

Fig.5: Variation of locus of multiply reflected field with the normalized length k_gL of secondary waveguide: (a) forward electric fields of No.2 secondary waveguide at the grill mouth, (b) reflected field of primary waveguide at the junction, where w=3.5cm, d=0.5cm, W=15.5cm, f=800MHz, $\Delta\phi$=90°, n_{wgd}/n_c=31.6 and $\nabla n_{wgd}=1 \times 10^{11} cm^{-4}$.

Fig.6: Schematic model to explain how a multijunction-grill field $\boldsymbol{E}$ caused by multiple reflections changes with k_gL. (a) variation in locus of $\boldsymbol{E}$ when the value of k_gL changes by

$k_g\Delta L$; we assume E is roughly expressed by $E^{(1)}+E^{(2)}$, where $E^{(1)} = |E^{(1)}|\angle k_g\Delta L$ and $E^{(2)} = |E^{(2)}|\angle(\vartheta + 3k_g\Delta L)$. (b) phase $\angle E$ and (c) amplitude $|E|$ versus $k_g\Delta L$ for ϑ=45° (solid curve) and 135° (dashed curve), where $|E^{(1)}|$=1 and $|E^{(2)}|$=0.6.

Fig.7: (a) Electric field reflection coefficient of primary waveguide as functions of phasing $\Delta\phi$ for various normalized length k_gL of secondary waveguide. (b) Directivity of power radiated from the grill mouth into plasma as functions of $\Delta\phi$ for various k_gL, where directivity is calculated by $\left(\int_1^{\infty} P(N_z)\,dN_z\right) \Big/ \left[\int_{-\infty}^{-1} P(N_z)\,dN_z + \int_1^{\infty} P(N_z)\,dN_z\right]$, w=3.5*cm*, d=0.5*cm*, W=15.5*cm*, f=800*MHz*, n_{wgd}/n_c=10 and $\nabla n_{wgd}=1\times10^{11}cm^{-4}$.

Fig.8: Power spectra of waves radiated from the grill mouth into plasma for various values of k_gL, where bold solid curves are for the equivalent conventional grill, and w=3.5*cm*, d=0.5*cm*, W=15.5*cm*, f=800*MHz*, $\Delta\phi$=30°, n_{wgd}/n_c=10 and $\nabla n_{wgd}=1\times10^{11}cm^{-4}$.

Fig.9: Elements of scattering matrix $\hat{T}$ at the grill mouth. (a) amplitude and (b) phase of first column elements. (c) amplitude and (d) phase of second column elements, where open circles denote experimental values and dots, connected with lines for convenience, does calculated ones under conditions that w=3.5*cm*, d=0.5*cm*, W=15.5*cm*, f=800*MHz*, n_{wgd}/n_c=31.6 and ∇n_{wgd}=5x10^9 ~$1\times10^{11}cm^{-4}$

Fig.10: Amplitude of electric fields both in primary and secondary waveguides versus normalized length k_gL of secondary waveguide, where all values are normalized to the amplitude $|E_{i0}|$ of forward wave in primary waveguide. Here, EXPERIMENT and CALCULATION denote experimentally measured results and theoretically calculated ones: (a), (d) reflected wave $|E_{r0}|$ in primary waveguide. (b), (e) forward waves $|E_{ip}|$ in secondary waveguides. (c), (d) reflected waves $|E_{rp}|$ in secondary waveguides, where dots, open circles, asterisks and triangles indicate the results for 1st, 2nd, 3rd and 4th secondary waveguide, respectively. Here, w=3.5*cm*, d=0.5*cm*, W=15.5*cm*, f=800*MHz*, $\Delta\phi$=30°, n_{wgd}/n_c=31.6 and $\nabla n_{wgd}=1\times10^{11}cm^{-4}$.

Fig.11: Phase of electric fields both in primary and secondary waveguides versus k_gL, where all phases are plotted as the difference from the phase $\angle E_{i0}$ of forward wave in the primary waveguide. (a), (d) reflected wave $\angle E_{r0}$ in the primary waveguide. (b), (e) forward

waves $\angle E_{ip}$ in secondary waveguides. (c), (d) reflected waves $\angle E_{rp}$ in secondary waveguides. The parameters are the same as those in Fig.10.

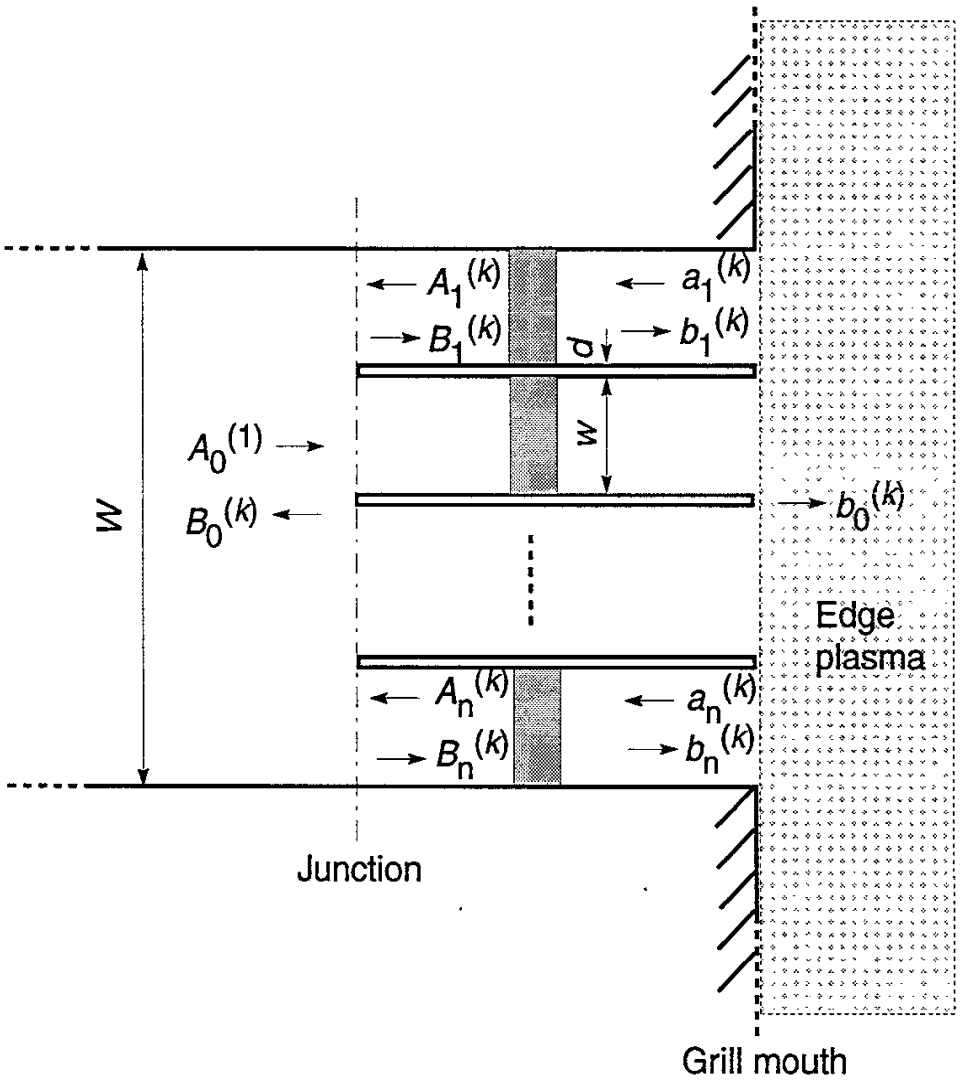
$A_1^{(k)}$
$a_1^{(k)}$
$B_1^{(k)}$
$b_1^{(k)}$
d
W
$A_0^{(1)}$
$B_0^{(k)}$
$b_0^{(k)}$
Edge plasma
$A_n^{(k)}$
$a_n^{(k)}$
$B_n^{(k)}$
$b_n^{(k)}$
Junction
Grill mouth

Fig.1 ⑨

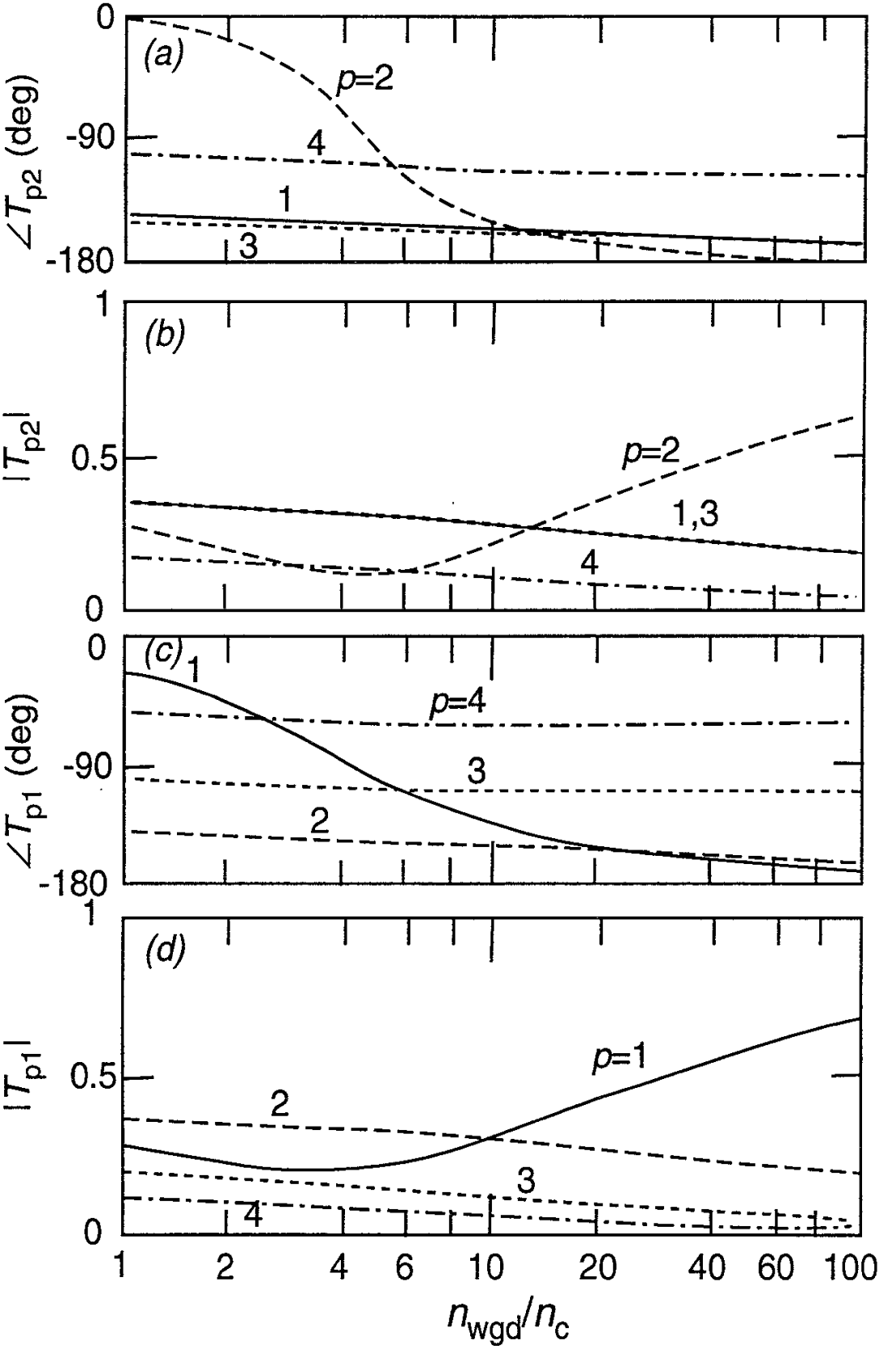
(a)
p=2
4
1
3
0
-90
-180
∠T_p2 (deg)
(b)
p=2
1,3
4
1
0.5
0
|T_p2|
(c)
1
p=4
3
2
0
-90
-180
∠T_p1 (deg)
(d)
p=1
2
3
4
1
0.5
0
|T_p1|
1
2
4
6
10
20
40
60
100
n_wgd/n_c

Fig.2

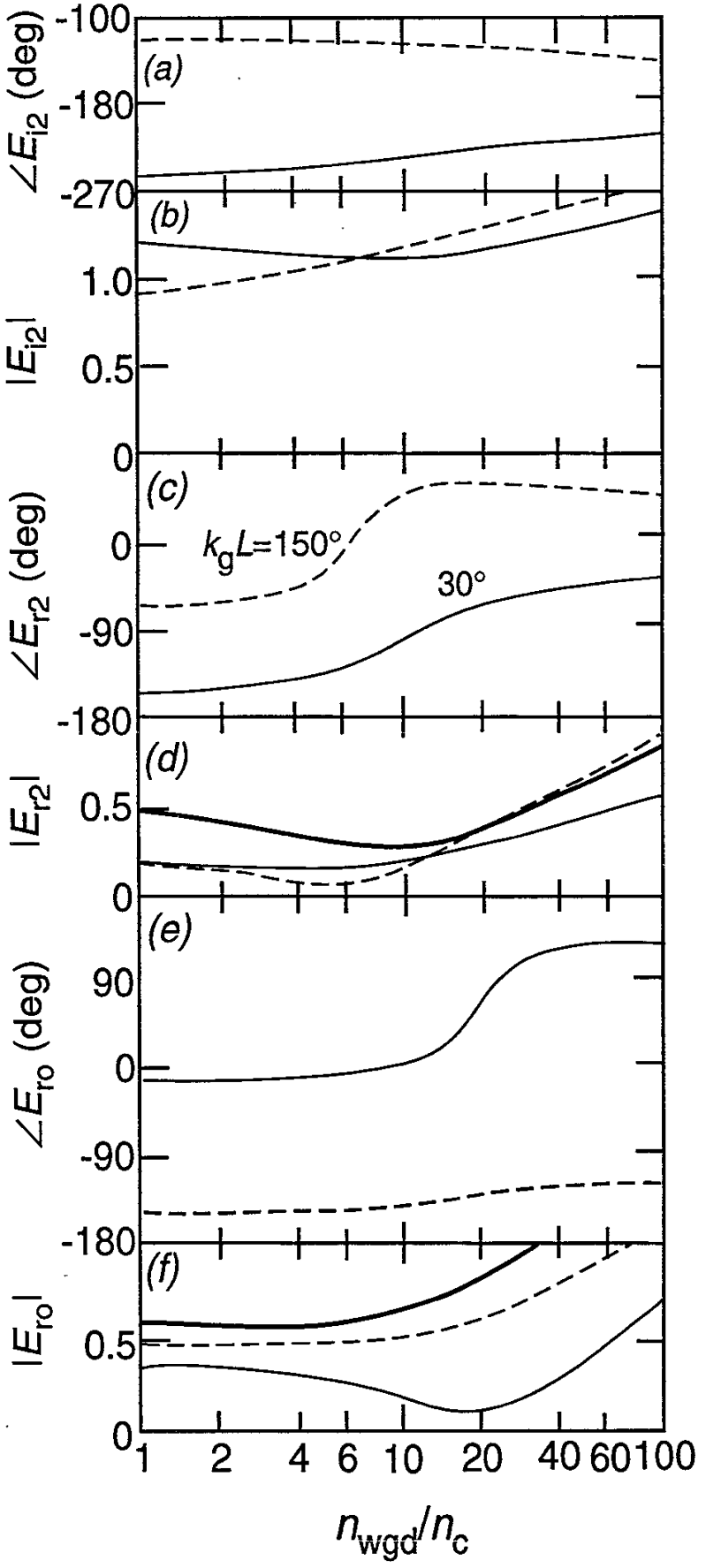
-100
-180
-270
(a)
∠E_i2 (deg)
(b)
1.0
0.5
0
|E_i2|
(c)
0
-90
-180
k_gL=150°
30°
∠E_r2 (deg)
(d)
0.5
0
|E_r2|
(e)
90
0
-90
-180
∠E_ro (deg)
(f)
0.5
0
|E_ro|
1
2
4
6
10
20
40
60
100
n_wgd/n_c

Fig.3

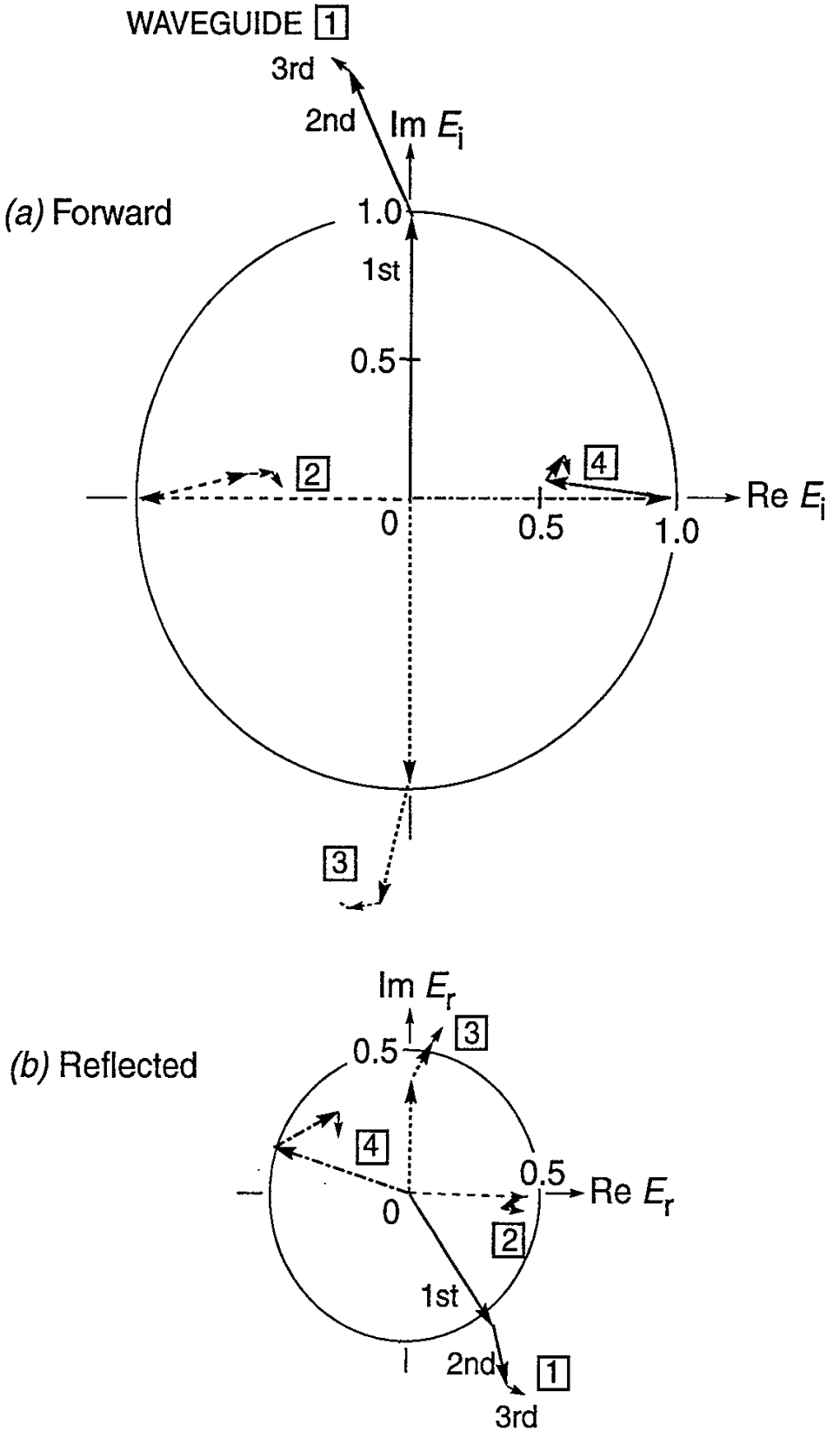
WAVEGUIDE 1
3rd
2nd
Im E_i
(a) Forward
1.0
1st
0.5
2
4
0
0.5
1.0
Re E_i
3
Im E_r
(b) Reflected
0.5
3
4
0.5
Re E_r
0
2
1st
2nd
1
3rd

Fig.4

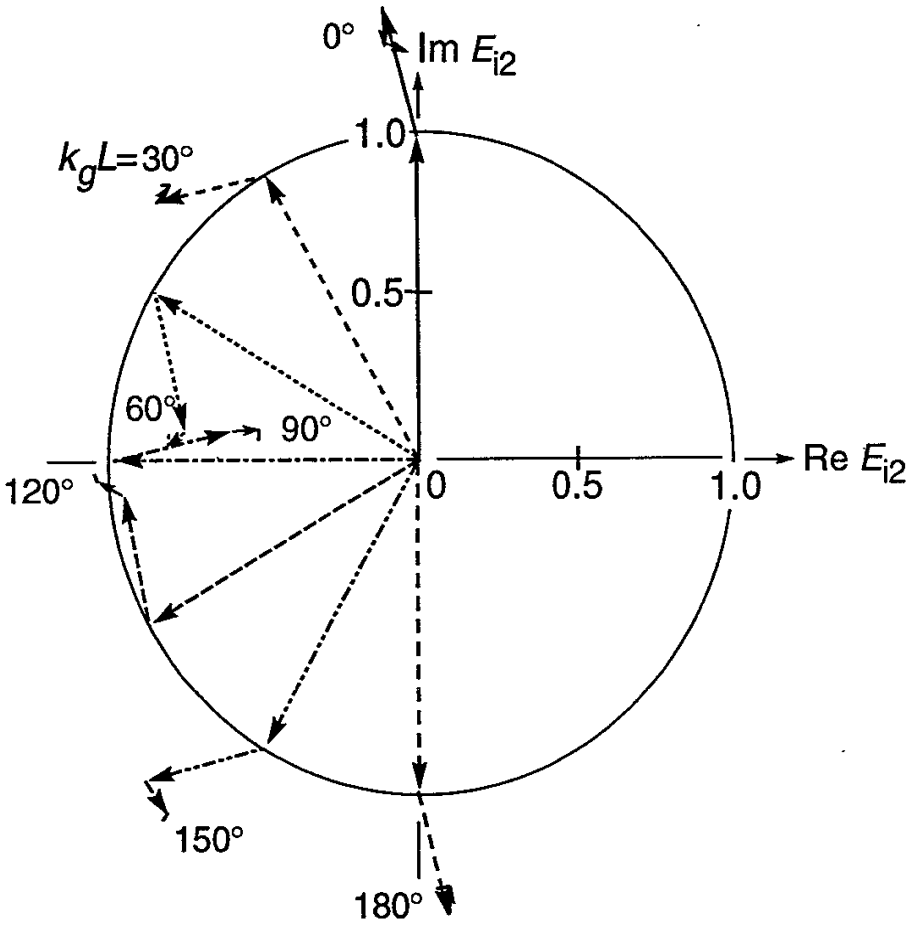

(a) Forward (No.2 SECONDARY WAVEGUIDE)

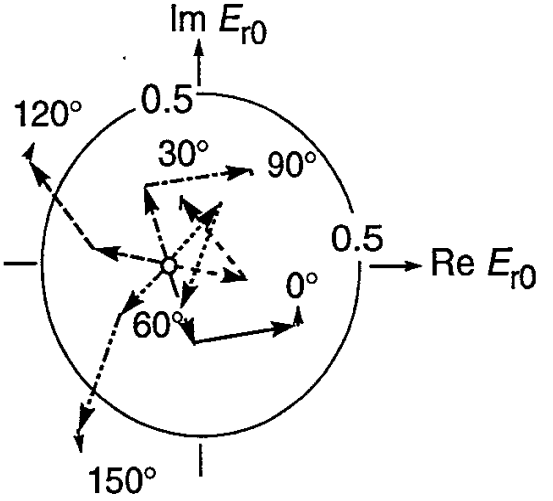

(b) Reflected (PRIMARY WAVEGUIDE)

Fig.5

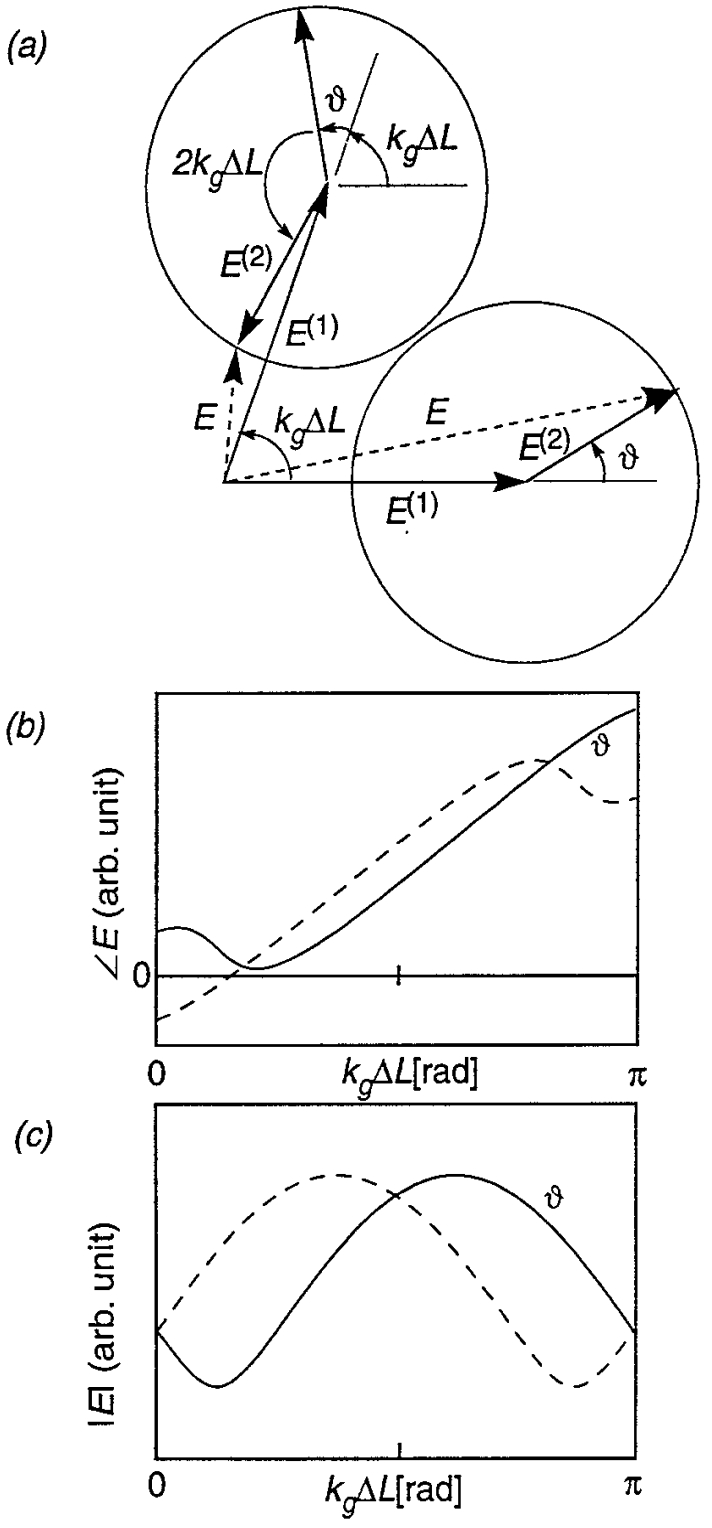
(a)
ϑ
$k_g\Delta L$
$2k_g\Delta L$
$E^{(2)}$
$E^{(1)}$
E
$k_g\Delta L$
E
$E^{(2)}$
ϑ
$E^{(1)}$
(b)
∠E (arb. unit)
ϑ
0
0
$k_g\Delta L$[rad]
π
(c)
|E| (arb. unit)
ϑ
0
$k_g\Delta L$[rad]
π

Fig.6

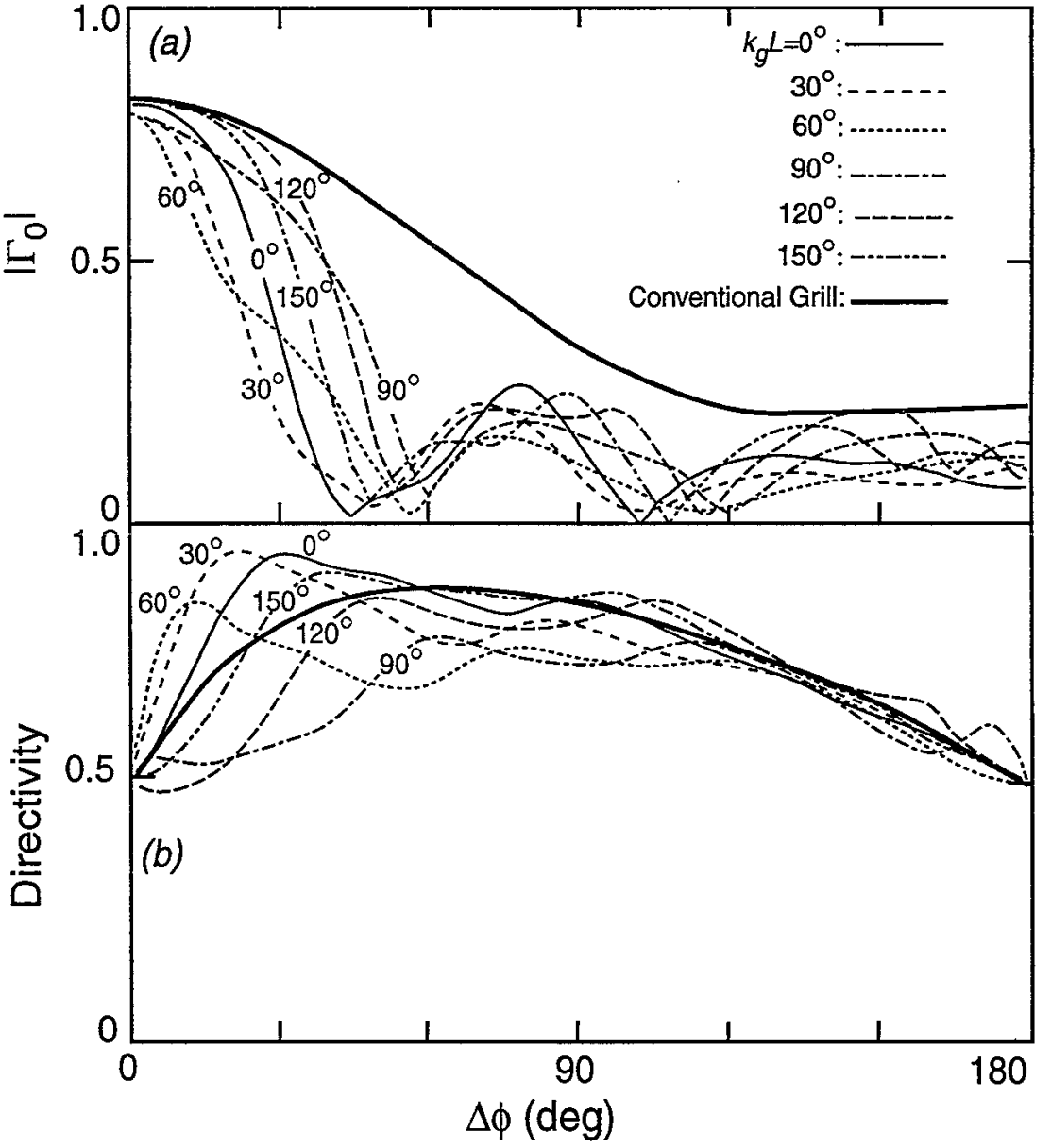
(a)
k_gL=0° :
30°:
60°:
90°:
120°:
150°:
Conventional Grill:
$|\Gamma_0|$
1.0
0.5
0
60°
120°
0°
150°
30°
90°
(b)
Directivity
30°
0°
60°
150°
120°
90°
0
90
180
Δϕ (deg)

Fig.7

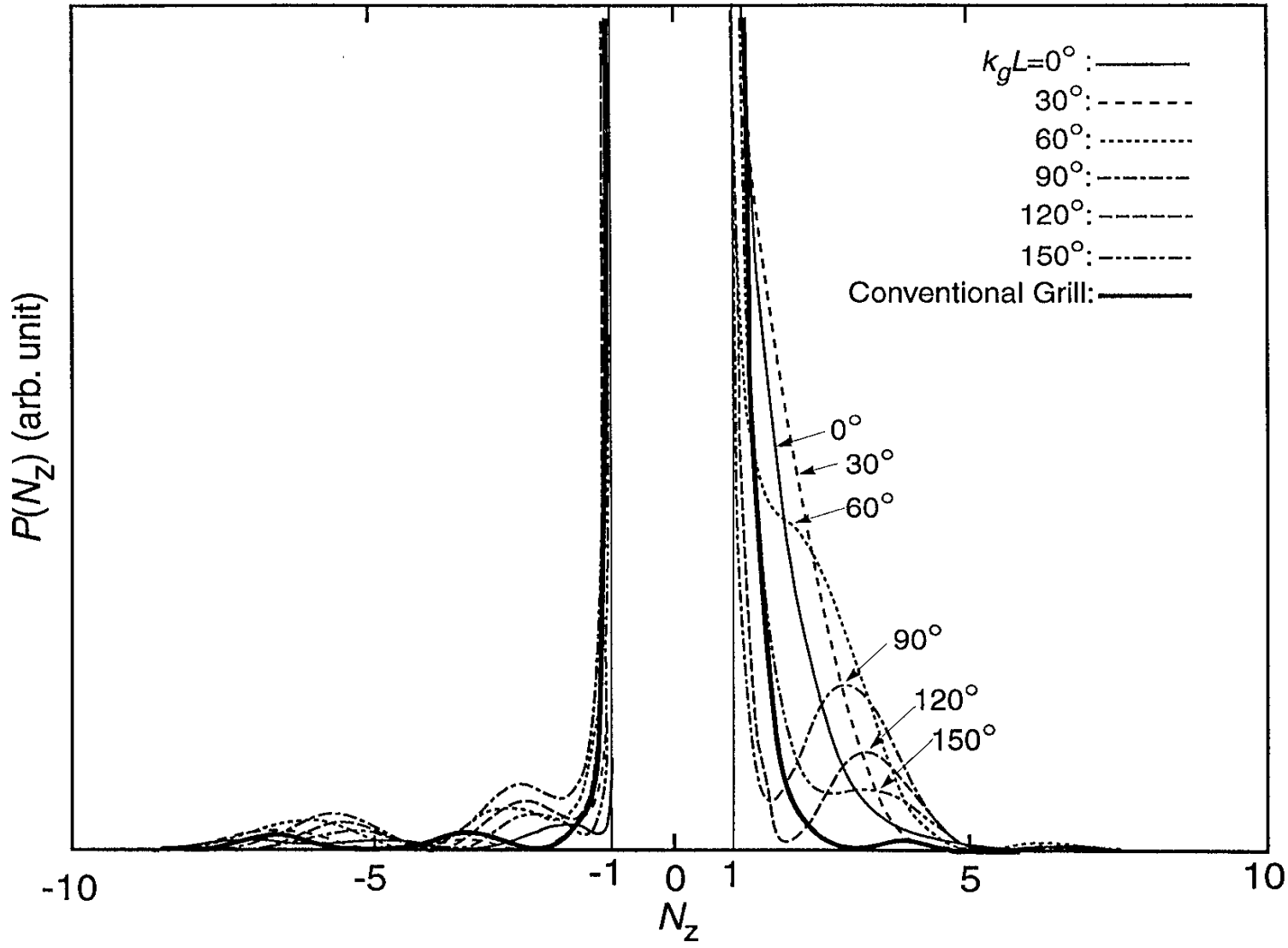
k_gL=0° :
30°:
60°:
90°:
120°:
150°:
Conventional Grill:
0°
30°
60°
90°
120°
150°
$P(N_Z)$ (arb. unit)
-10
-5
-1
0
1
5
10
N_z

Fig.8

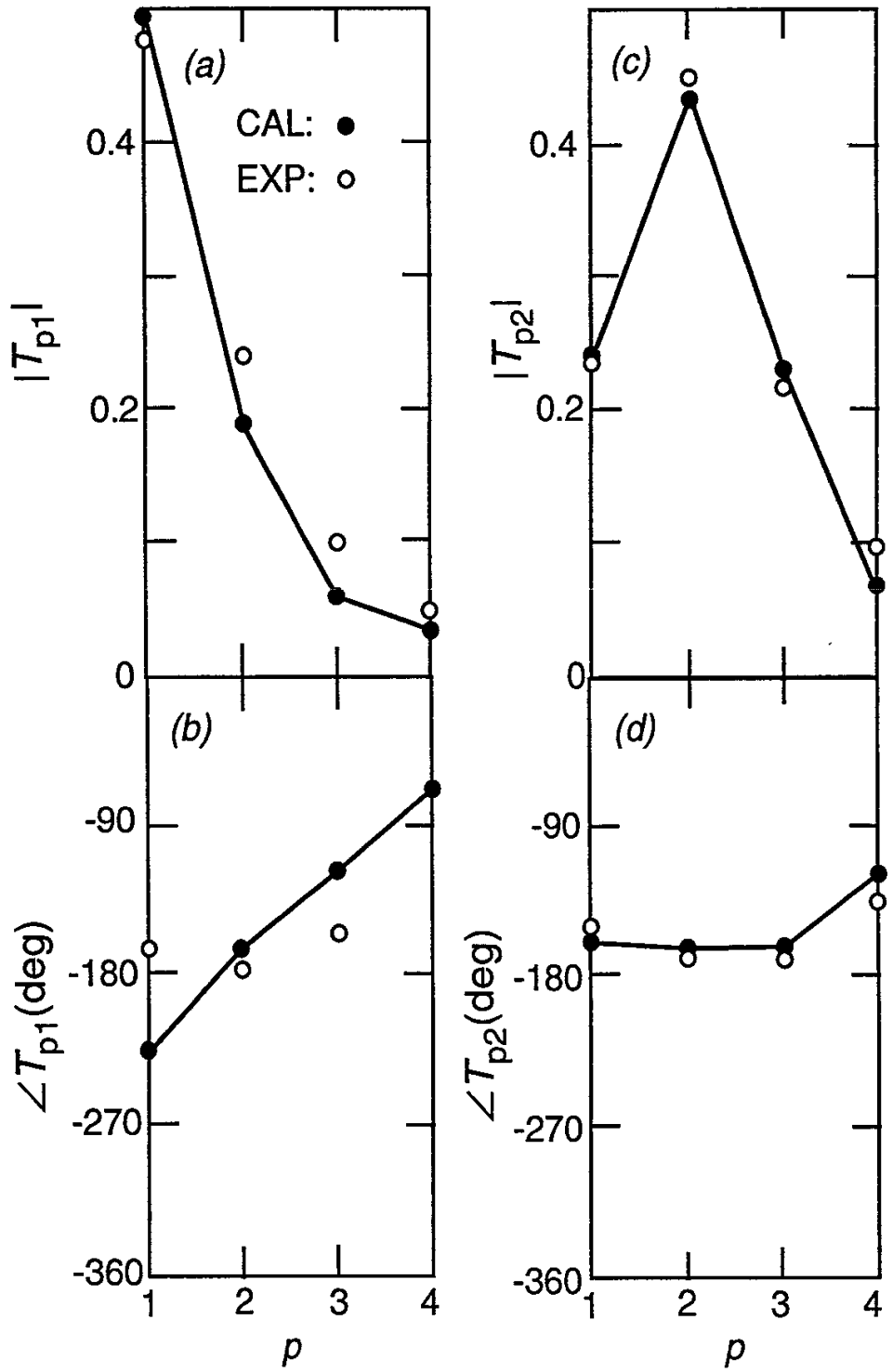
(a)
CAL:
EXP:
0.4
0.2
0
$|T_{p1}|$
(b)
-90
-180
-270
-360
$\angle T_{p1}$(deg)
1
2
3
4
p
(c)
0.4
0.2
0
$|T_{p2}|$
(d)
-90
-180
-270
-360
$\angle T_{p2}$(deg)
1
2
3
4
p

Fig.9

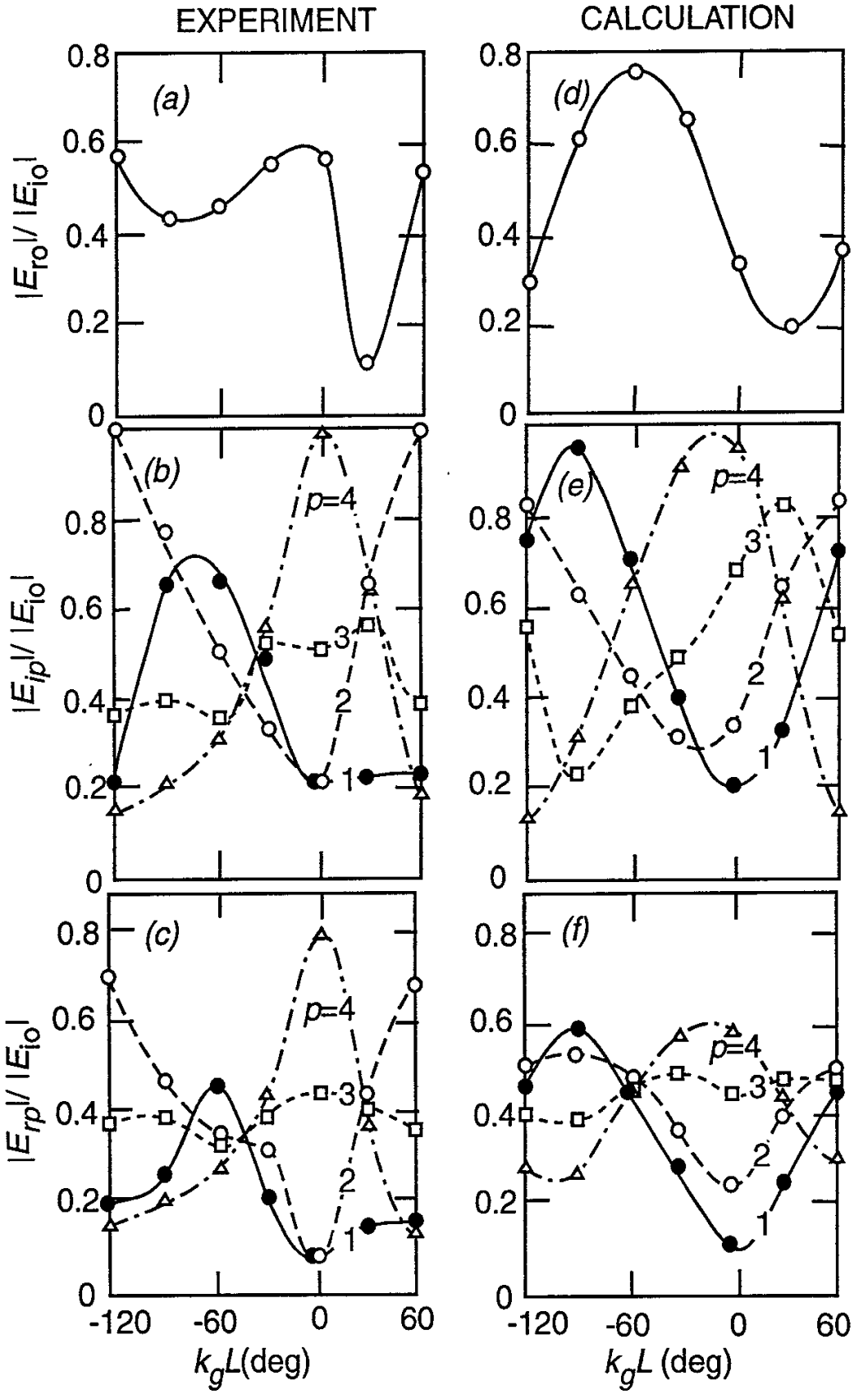
EXPERIMENT
CALCULATION
(a)
(b)
(c)
(d)
(e)
(f)
$|E_{ro}|/|E_{io}|$
$|E_{ip}|/|E_{io}|$
$|E_{rp}|/|E_{io}|$
p=4
3
2
1
0.8
0.6
0.4
0.2
0
-120
-60
0
60
k_gL(deg)
k_gL (deg)

Fig.10

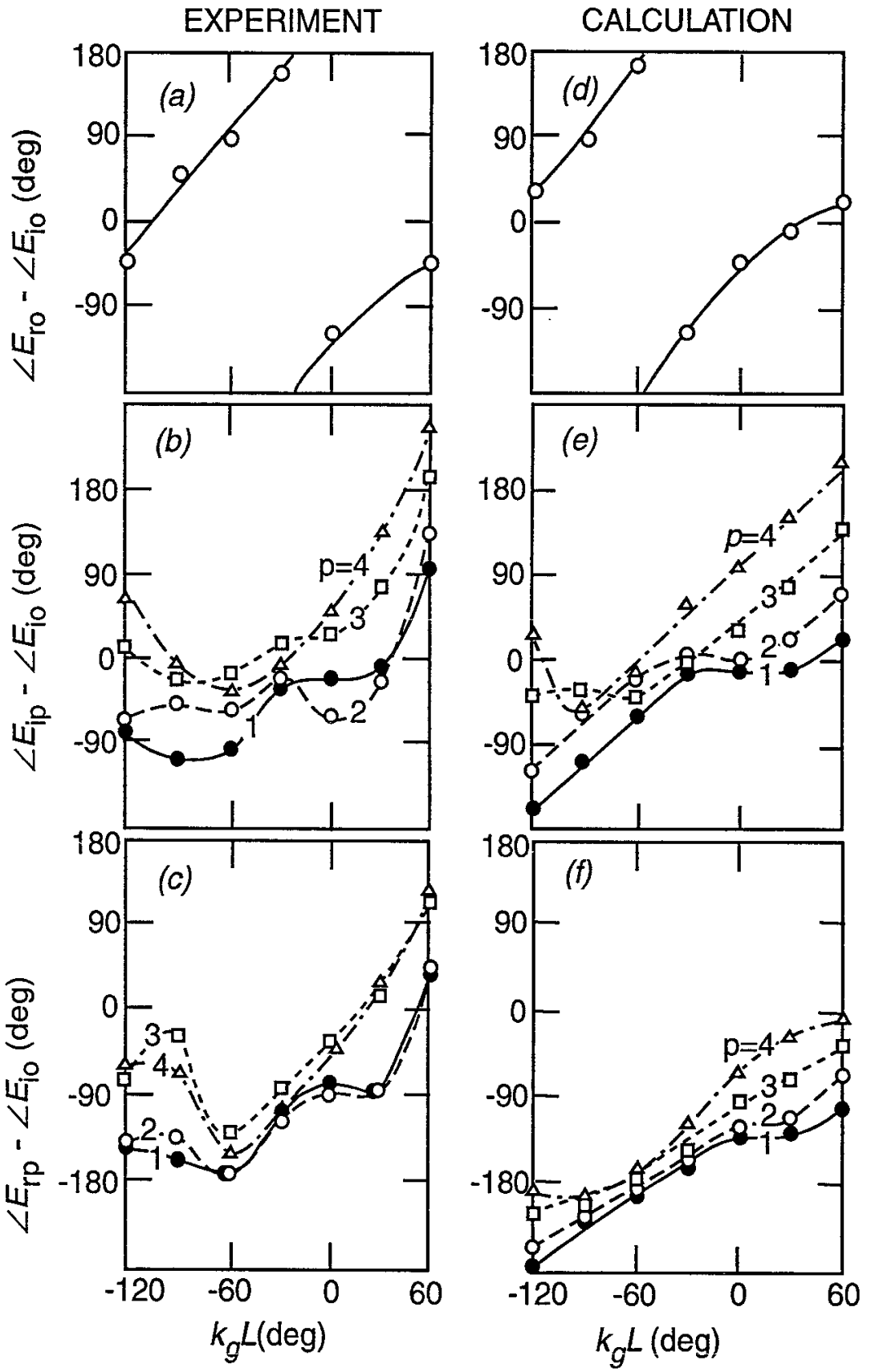
EXPERIMENT
CALCULATION
(a)
(b)
(c)
(d)
(e)
(f)
180
90
0
-90
-180
-120
-60
60
p=4
3
2
1
4
$\angle E_{ro} - \angle E_{io}$ (deg)
$\angle E_{ip} - \angle E_{io}$ (deg)
$\angle E_{rp} - \angle E_{io}$ (deg)
$k_g L$(deg)
$k_g L$ (deg)

Fig.11

Recent Issues of NIFS Series

NIFS-94 H. Sanuki, K. Itoh, K. Ida and S. - I. Itoh, *On Radial Electric Field Structure in CHS Torsatron / Heliotron;* Jun. 1991

NIFS-95 K. Itoh, H. Sanuki and S. - I. Itoh, *Influence of Fast Ion Loss on Radial Electric Field in Wendelstein VII-A Stellarator;* Jun. 1991

NIFS-96 S. - I. Itoh, K. Itoh, A. Fukuyama, *ELMy-H mode as Limit Cycle and Chaotic Oscillations in Tokamak Plasmas;* Jun. 1991

NIFS-97 K. Itoh, S. - I. Itoh, H. Sanuki, A. Fukuyama, *An H-mode-Like Bifurcation in Core Plasma of Stellarators;* Jun. 1991

NIFS-98 H. Hojo, T. Watanabe, M. Inutake, M. Ichimura and S. Miyoshi, *Axial Pressure Profile Effects on Flute Interchange Stability in the Tandem Mirror GAMMA 10;* Jun. 1991

NIFS-99 A. Usadi, A. Kageyama, K. Watanabe and T. Sato, *A Global Simulation of the Magnetosphere with a Long Tail : Southward and Northward IMF;* Jun. 1991

NIFS-100 H. Hojo, T. Ogawa and M. Kono, *Fluid Description of Ponderomotive Force Compatible with the Kinetic One in a Warm Plasma* ; July 1991

NIFS-101 H. Momota, A. Ishida, Y. Kohzaki, G. H. Miley, S. Ohi, M. Ohnishi K. Yoshikawa, K. Sato, L. C. Steinhauer, Y. Tomita and M. Tuszewski *Conceptual Design of D-^{3}He FRC Reactor "ARTEMIS"* ; July 1991

NIFS-102 N. Nakajima and M. Okamoto, *Rotations of Bulk Ions and Impurities in Non-Axisymmetric Toroidal Systems* ; July 1991

NIFS-103 A. J. Lichtenberg, K. Itoh, S. - I. Itoh and A. Fukuyama, *The Role of Stochasticity in Sawtooth Oscillation* ; Aug. 1991

NIFS-104 K. Yamazaki and T. Amano, *Plasma Transport Simulation Modeling for Helical Confinement Systems;* Aug. 1991

NIFS-105 T. Sato, T. Hayashi, K. Watanabe, R. Horiuchi, M. Tanaka, N. Sawairi and K. Kusano, *Role of Compressibility on Driven Magnetic Reconnection ;* Aug. 1991

NIFS-106 Qian Wen - Jia, Duan Yun - Bo, Wang Rong - Long and H. Narumi, *Electron Impact Excitation of Positive Ions - Partial Wave Approach in Coulomb - Eikonal Approximation* ; Sep. 1991

NIFS-107 S. Murakami and T. Sato, *Macroscale Particle Simulation of Externally Driven Magnetic Reconnection;* Sep. 1991

NIFS-108 Y. Ogawa, T. Amano, N. Nakajima, Y. Ohyabu, K. Yamazaki, S. P. Hirshman, W. I. van Rij and K. C. Shaing, *Neoclassical Transport Analysis in the Banana Regime on Large Helical Device (LHD) with the DKES Code;* Sep. 1991

NIFS-109 Y. Kondoh, *Thought Analysis on Relaxation and General Principle to Find Relaxed State;* Sep. 1991

NIFS-110 H. Yamada, K. Ida, H. Iguchi, K. Hanatani, S. Morita, O. Kaneko, H. C. Howe, S. P. Hirshman, D. K. Lee, H. Arimoto, M. Hosokawa, H. Idei, S. Kubo, K. Matsuoka, K. Nishimura, S. Okamura, Y. Takeiri, Y. Takita and C. Takahashi, *Shafranov Shift in Low-Aspect-Ratio Heliotron / Torsatron CHS* ; Sep 1991

NIFS-111 R. Horiuchi, M. Uchida and T. Sato, *Simulation Study of Stepwise Relaxation in a Spheromak Plasma ;* Oct. 1991

NIFS-112 M. Sasao, Y. Okabe, A. Fujisawa, H. Iguchi, J. Fujita, H. Yamaoka and M. Wada, *Development of Negative Heavy Ion Sources for Plasma Potential Measurement* ; Oct. 1991

NIFS-113 S. Kawata and H. Nakashima, *Tritium Content of a DT Pellet in Inertial Confinement Fusion* ; Oct. 1991

NIFS-114 M. Okamoto, N. Nakajima and H. Sugama, *Plasma Parameter Estimations for the Large Helical Device Based on the Gyro-Reduced Bohm Scaling* ; Oct. 1991

NIFS-115 Y. Okabe, *Study of Au^- Production in a Plasma-Sputter Type Negative Ion Source* ; Oct. 1991

NIFS-116 M. Sakamoto, K. N. Sato, Y. Ogawa, K. Kawahata, S. Hirokura, S. Okajima, K. Adati, Y. Hamada, S. Hidekuma, K. Ida, Y. Kawasumi, M. Kojima, K. Masai, S. Morita, H. Takahashi, Y. Taniguchi, K. Toi and T. Tsuzuki, *Fast Cooling Phenomena with Ice Pellet Injection in the JIPP T-IIU Tokamak;* Oct. 1991

NIFS-117 K. Itoh, H. Sanuki and S. -I. Itoh, *Fast Ion Loss and Radial Electric Field in Wendelstein VII-Λ Stellarator*; Oct. 1991

NIFS-118 Y. Kondoh and Y. Hosaka, *Kernel Optimum Nearly-analytical Discretization (KOND) Method Applied to Parabolic Equations <<KOND-P Scheme>>;* Nov. 1991

NIFS-119 T. Yabe and T. Ishikawa, *Two- and Three-Dimensional Simulation Code for Radiation-Hydrodynamics in ICF*; Nov. 1991

NIFS-120 S. Kawata, M. Shiromoto and T. Teramoto, *Density-Carrying Particle Method for Fluid* ; Nov. 1991

NIFS-121 T. Ishikawa, P. Y. Wang, K. Wakui and T. Yabe, *A Method for the High-speed Generation of Random Numbers with Arbitrary Distributions;* Nov. 1991

NIFS-122 K. Yamazaki, H. Kaneko, Y. Taniguchi, O. Motojima and LHD Design *Group, Status of LHD Control System Design ; Dec. 1991*

NIFS-123 Y. Kondoh, *Relaxed State of Energy in Incompressible Fluid and Incompressible MHD Fluid* ; Dec. 1991

NIFS-124 K. Ida, S. Hidekuma, M. Kojima, Y. Miura, S. Tsuji, K. Hoshino, M. Mori, N. Suzuki, T. Yamauchi and JFT-2M Group, *Edge Poloidal Rotation Profiles of H-Mode Plasmas in the JFT-2M Tokamak ;* Dec. 1991

NIFS-125 H. Sugama and M. Wakatani, *Statistical Analysis of Anomalous Transport in Resistive Interchange Turbulence* ;Dec. 1991

NIFS-126 K. Narihara, *A Steady State Tokamak Operation by Use of Magnetic Monopoles* ; Dec. 1991

NIFS-127 K. Itoh, S. -I. Itoh and A. Fukuyama, *Energy Transport in the Steady State Plasma Sustained by DC Helicity Current Drive* ;Jan. 1992

NIFS-128 Y. Hamada, Y. Kawasumi, K. Masai, H. Iguchi, A. Fujisawa, JIPP T-IIU Group and Y. Abe, *New Hight Voltage Parallel Plate Analyzer* ; Jan. 1992

NIFS-129 K. Ida and T. Kato, *Line-Emission Cross Sections for the Charge-exchange Reaction between Fully Stripped Carbon and Atomic Hydrogen in Tokamak Plasma*; Jan. 1992

NIFS-130 T. Hayashi, A. Takei and T. Sato, *Magnetic Surface Breaking in 3D MHD Equilibria of l=2 Heliotron* ; Jan. 1992

NIFS-131 K. Itoh, K. Ichiguchi and S. -I. Itoh, *Beta Limit of Resistive Plasma in Torsatron/Heliotron* ; Feb. 1992

NIFS-132 K. Sato and F. Miyawaki, *Formation of Presheath and Current-Free Double Layer in a Two-Electron-Temperature Plasma* ; Feb. 1992

NIFS-133 T. Maruyama and S. Kawata, *Superposed-Laser Electron Acceleration* Feb. 1992

NIFS-134 Y. Miura, F. Okano, N. Suzuki, M. Mori, K. Hoshino, H. Maeda, T. Takizuka, JFT-2M Group, S.-I. Itoh and K. Itoh, *Rapid Change of Hydrogen Neutral Energy Distribution at L/H-Transition in JFT-2M H-mode ;* Feb. 1992

NIFS-135 H. Ji, H. Toyama, A. Fujisawa, S. Shinohara and K. Miyamoto *Fluctuation and Edge Current Sustainment in a Reversed-Field-Pinch;* Feb. 1992

NIFS-136 K. Sato and F. Miyawaki, *Heat Flow of a Two-Electron-Temperature Plasma through the Sheath in the Presence of Electron Emission;* Mar. 1992

NIFS-137 T. Hayashi, U. Schwenn and E. Strumberger, *Field Line Diversion Properties of Finite ß Helias Equilibria;* Mar. 1992

NIFS-138 T. Yamagishi, *Kinetic Approach to Long Wave Length Modes in Rotating Plasmas;* Mar. 1992

NIFS-139 K. Watanabe, N. Nakajima, M. Okamoto, Y. Nakamura and M. Wakatani, *Three-dimensional MHD Equilibrium in the Presence of Bootstrap Current for Large Helical Device (LHD);* Mar. 1992

NIFS-140 K. Itoh, S. -I. Itoh and A. Fukuyama, *Theory of Anomalous Transport in Toroidal Helical Plasmas;* Mar. 1992

NIFS-141 Y. Kondoh, *Internal Structures of Self-Organized Relaxed States and Self-Similar Decay Phase;* Mar. 1992

NIFS-142 U. Furukane, K. Sato, K. Takiyama and T. Oda, *Recombining Processes in a Cooling Plasma by Mixing of Initially Heated Gas;* Mar. 1992

NIFS-143 Y. Hamada, K. Masai, Y. Kawasumi, H. Iguchi, A. Fijisawa and JIPP T-IIU Group, *New Method of Error Elimination in Potential Profile Measurement of Tokamak Plasmas by High Voltage Heavy Ion Beam Probes;* Apr. 1992

NIFS-144 N. Ohyabu, N. Noda, Hantao Ji, H. Akao, K. Akaishi, T. Ono, H. Kaneko, T. Kawamura, Y. Kubota, S. Morimoto. A. Sagara, T. Watanabe, K. Yamazaki and O. Motojima, *Helical Divertor in the Large Helical Device;* May 1992